WATER RESOURCES RESEARCH, VOL. 23, NO. 10, PAGES 1851–1866, OCTOBER 1987

Variable Density Flow and Solute Transport Simulation of Regional Aquifers Containing a Narrow Freshwater-Saltwater Transition Zone

CLIFFORD I. VOSS

U.S. Geological Survey, Reston, Virginia

WILLIAM R. SOUZA

U.S. Geological Survey, Honolulu, Hawaii

Variable density flow and solute transport simulation of aquifer systems containing narrow transition zones between freshwater and saltwater requires particular attention to certain aspects of the numerical method and its application to be successful. Typically, only cases involving wide transition zones have been simulated with variable density transport models, possibly because of inaccuracies in the modeling approaches used. The major components of a successful approach are threefold. First, functionally consistent approximation of terms involved in fluid velocity calculations is necessary. In the case of Galerkin finite element methodology, a significant modification is required to the standard approach in order to achieve consistency. Second, the simulator must be verified in a particular series of tests. The usual tests using Henry's problem for verification of density-dependent transport simulators are inadequate to check for consistency of the velocity approximations and for the accuracy of simulating flow driven by bouyancy forces. Third, adequately fine spatial discretization is required when applying the simulator for spatial stability of the numerical transport solution and to allow accurate representation of narrow transition zones and the effects of low transverse dispersivity. The effectiveness of this approach is demonstrated through simulation of the flow of fresh and saline groundwater in the layered basalt aquifer of southern Oahu, Hawaii. The transition zone in this regional flow system is narrow except near the discharge area where it is broadly dispersed. Simulation of this common situation with an inconsistent approximation gives grossly incorrect results, while simulation with a consistent model provides a robust tool for analysis of system hydrology.

INTRODUCTION

The problem in analyzing a regional aquifer system containing a narrow transition zone between freshwater and saltwater with a variable density fluid flow and dissolved solids transport model is twofold.

1. The adequacy of the Fickian dispersion theory is not certain, and values of dispersion parameters are neither well-known nor may they be directly measured at the regional scale. The physical basis of a particular concentration transition zone structure may be studied only after careful fitting of simulated hydraulics to the field conditions. This requires that the transport simulation accurately represent the physical governing equations before evaluation of the adequacy of old and new dispersion models and the determination of parameter values at the field scale can be undertaken.

2. Transport codes, however, have considerable difficulties simulating the movement of narrow concentration fronts on a regional scale. The difficulties are (1) spatial instabilities in the numerical concentration solution when tracking a narrow front, (2) inability to maintain the narrowness of a front due to insufficient discretization, (3) significant numerical errors in calculating fluid velocity within narrow transition zones causing broadening of the zones, and (4) inaccuracies in representation of bulk fluid movement driven by density differences.

Classically, the problems inherent in transport simulation of freshwater-saltwater systems containing portions of narrow transition zones are skirted by basing the analysis on a variety of sharp interface approximations. The various areal and cross-sectional approaches are reviewed by *Reilly and Goodman* [1985]. While not minimizing the great value of such approaches in representing fundamental aspects of aquifer system dynamics, they do not account for the often significant effect of the mixing process on the structure and position of the transition zone, nor do they allow a means of direct prediction of the dissolved solids concentration of water arriving at supply wells. The impact of these limitations is clear when considering that water of potable quality contains less than about one percent seawater. On the other hand, regional scale analysis based on variable density flow and transport simulation is capable of representing system dynamics including the effects of mixing, as founded on current theories of dispersion in aquifers, and is capable of making predictions of concentration.

Often in regional aquifers, the transition zone is relatively narrow except in areas that undergo pumping, recharge, discharge, or tidal stresses. The ability to simultaneously simulate the dynamics of both narrow and broad portions of the transition zone is vital to hydrologic analysis and water supply prediction in such cases. However, transport simulations have almost exclusively dealt with transition zones that are quite broad on the regional scale (on the order of aquifer thickness or greater). These include analyses reported by *Lee and Cheng* [1974], *Segol and Pinder* [1976], *Volker and Rushton* [1982], *Frind* [1982*b*], and *Lebbe* [1983]. Some authors [*Volker*, 1980; *Frind*, 1982*a*] have shown results for narrower transi-

Paper number 6W4664.

tion zones. Speculation may be warranted, however, on the question of whether broad transition zones are often chosen as candidates for transport simulation analysis because of the numerical problems in representing narrow zones, and further, whether in some cases, inaccuracies in variable density transport models give broad transition results that are accepted for lack of definitive field data showing otherwise.

This paper describes a numerical modeling approach that deals with the above-mentioned problems in representation of freshwater and saltwater systems. The approch guarantees adequate regional scale transport simulation of narrow transition zones with minimal numerical dispersion. Through application of the modeling technique to the southern Oahu aquifer, Oahu, Hawaii, it is demonstrated that transport simulation can provide an excellent tool for hydraulic investigation even when narrow transition zones are involved.

THEORY

The solute mass balance per unit aquifer volume at a point in an aquifer cross section with variable density fluid is given by [*Bear*, 1979]

$$\varepsilon\rho \frac{\partial C}{\partial t} + \varepsilon\rho \mathbf{v} \cdot \nabla C - \nabla \cdot [\varepsilon\rho(D_m \mathbf{I} + \mathbf{D}) \cdot \nabla C] = Q_p(C^* - C) \quad (1)$$

where

- $C(x, z, t)$ solute concentration as a mass fraction, (mass solute/mass fluid) in units M_s/M, where M_s are units of solute mass and M are units of fluid mass;
- $\varepsilon(x, z)$ aquifer volumetric porosity, 1;
- $\mathbf{v}(x, z, t)$ fluid velocity, in units L/T, where L are length units and T are time units;
- D_m the molecular diffusion coefficient of solute in pure fluid including aquifer material tortuosity effects, L^2/T;
- $\mathbf{I}$ identity tensor, 1;
- $\mathbf{D}(x, z, t)$ mechanical dispersion tensor, L^2/T;
- $Q_p(x, z, t)$ fluid mass source (mass fluid/aquifer volume/time) $M/L^3\ T$;
- $C^*(x, z, t)$ concentration of solute as a mass fraction in the source fluid, M_s/M;
- $\rho(x, z, t)$ fluid density, $M/L_f{}^3$, where $L_f{}^3$ is fluid volume.

Density is given as a linear function of concentration:

$$\rho = \rho_0 + \frac{\partial \rho}{\partial C}(C - C_0) \quad (2)$$

where ρ_0 is fluid density when $C = C_0$; C_0 is a base solute concentration; and $\partial\rho/\partial C$ is a constant coefficient of density variability.

Darcy's law gives the mass average fluid velocity at any point in a cross section as

$$\mathbf{v} = -\left(\frac{\mathbf{k}}{\varepsilon\mu}\right) \cdot (\nabla p - \rho \mathbf{g}) \quad (3)$$

where

- $\mathbf{k}(x, z)$ permeability tensor, L^2;
- μ fluid dynamic viscosity, M/LT;
- $\mathbf{g}$ gravity vector, L/T^2;
- $p(x, z, t)$ fluid pressure, M/LT^2.

The mass balance of fluid per unit aquifer volume at a point in the aquifer, assuming the contribution of solute dispersion to the mass average flux of fluid is negligible, may be given by [*Bear*, 1979]

$$\rho S_{op} \frac{\partial p}{\partial t} + \varepsilon \frac{\partial \rho}{\partial C} \frac{\partial C}{\partial t} + \nabla \cdot (\varepsilon\rho \mathbf{v}) = Q_p \quad (4)$$

into which Darcy's law (3) for mass average velocity may be substituted. The specific pressure storativity S_{op} for a rigid solid aquifer matrix $(M/(LT^2))^{-1}$ is given by

$$S_{op} = (1 - \varepsilon)\alpha + \varepsilon\beta \quad (5)$$

where α is porous matrix compressibility $(M/(LT^2))^{-1}$, and β is fluid compressibility $(M/(LT^2))^{-1}$.

A general boundary condition for the fluid mass balance that applies at stationary boundaries as well as approximately at a water table (see *Bear* [1979, pp. 98–99] and Appendix B for development of similar conditions) is

$$\frac{S_y}{|g|} \frac{\partial p}{\partial t} + \varepsilon\rho \mathbf{v} \cdot \mathbf{n} + Q_{IN}{}^* = 0 \quad (6)$$

where

- $S_y(x, z)$ water table specific yield (volume fluid released/aquifer volume) for unit drop in hydraulic head, 1;
- $|g|$ magnitude of gravitational acceleration, L/T^2;
- $Q_{IN}{}^*$ fluid mass source due to flow across boundaries (mass fluid recharged per unit area of boundary/time) M/L^2T.
- $\mathbf{n}$ unit outward normal to the boundary, 1.

This condition is accurate when at a water table, $|\nabla\rho| \approx \rho|g|$, that is, when pressure gradients are nearly hydrostatic at the water table. This condition is usually satisfied because commonly vertical pressure gradients are nearly hydrostatic and horizontal gradients are much smaller than vertical gradients.

The mechanical dispersion tensor for an isotropic porous medium in two spatial dimensions is given by

$$\mathbf{D} = \begin{bmatrix} D_{xx} & D_{xz} \\ D_{zx} & D_{zz} \end{bmatrix} \quad (7)$$

where

$$D_{xx} = \left(\frac{1}{|v^2|}\right)(d_L v_x{}^2 + d_T v_z{}^2) \quad (8)$$

$$D_{zz} = \left(\frac{1}{|v^2|}\right)(d_T v_x{}^2 + d_L v_z{}^2) \quad (9)$$

$$D_{xz} = D_{zx} = \left(\frac{1}{|v^2|}\right)(d_L - d_T)(v_x v_z) \quad (10)$$

$$d_L = \alpha_L |v| \quad (11)$$

$$d_T = \alpha_T |v| \quad (12)$$

where $|v|$ is the magnitude of velocity and d_L and d_T are longitudinal and transverse coefficients of mechanical dispersion L^2/T, and $\alpha_L(x, z)$ is longitudinal dispersivity, L, and $\alpha_T(x, z)$ is transverse dispersivity, L.

NUMERICAL METHOD WITH CONSISTENT VELOCITIES

The first component of a successful approach to simulation of variable density fluid movement is a consistent velocity approximation. While the general conclusions of the following

discussion on this topic are applicable to any numerical method, the ideas are developed on the basis of the finite element method. A weighted residual numerical method combining Galerkin finite elements with integrated finite differences described in Appendix A is used to solve the two governing equations, (1) and (4). The Galerkin finite element method allows great geometric flexibility in mesh design and gives robust direction- and anisotropy-independent representation of fluid and solute fluxes. An integrated finite difference approximation for the spatial integration of all nonflux terms in the governing equations provides an economical alternative to the Galerkin method while giving accuracy sufficient for any mildly nonlinear simulation problem. A backward finite difference approximation discretizes the time derivatives. Upstream weighted methods for the transport equation solution are not used, for reasons discussed in Appendix A.

The variables, pressure $p(x, z, t)$, and concentration $C(x, z, t)$, are discretized as a piecewise continuous function in space using bilinear basis functions on quadrilateral finite elements. Their value at any point (x, z, t) is assumed to be constant in the y direction, as the model is two dimensional. This is expressed for a mesh with NN nodes as

$$p(x, z, t) \approx \sum_{i=1}^{NN} p_i(t)\phi_i(x, z) \tag{13}$$

$$C(x, z, t) \approx \sum_{i=1}^{NN} C_i(t)\phi_i(x, z) \tag{14}$$

where $p_i(t)$ and $C_i(t)$ are the values of pressure and concentration at node i, and $\phi_i(x, z)$ is the basis function defined at node i. The basis function also is defined to take on a constant value for all y at a point (x, z) and is given by the expressions in Appendix B. The weighted residual numerical method is described in Appendix A.

Velocities must be evaluated throughout the simulated region for any numerical method. For the method in Appendix A, velocities must be evaluated within each finite element in order to carry out the integrations that arise. In particular, when using Gaussian integration, values of velocity are required at each Gauss point to complete the integration of the solute advection term. Velocity values are also required to calculate the velocity-dependent dispersion tensor. Fluid velocities based on the piecewise continuous pressure of relation (13) are continuous within each finite element and discontinuous at element boundaries. This is due to the discontinuity of discretized pressure gradients at element boundaries. Velocity $\mathbf{v}_i$ at a point (x_i, z_i) in an element is based on Darcy's law (equation 3) and is usually given by [e.g., *Pinder and Gray*, 1977, pp. 171–173; *Huyakorn and Pinder*, 1983, pp. 197–205]

$$\mathbf{v}_i = -\left(\frac{\mathbf{k}_i}{\varepsilon_i \mu_i}\right) \cdot \left(\sum_{k=1}^{4} p_k \nabla \phi_k + \rho_i |g| \nabla E\right) \tag{15}$$

where the k subscript ranges over the four nodes in the element and E is the elevation of the point above datum.

A functional inconsistency in this approximation which gives rise to artificial vertical velocities occurs in the case where both pressure and density are allowed to vary linearly (or have the same order in space) in the vertical direction across an element. This inconsistency may be the reason for previous difficulties with finite element simulators solving for pressure and concentration which employ velocities that are discontinuous from element to element [e.g., *Segol et al.*, 1975]. This inconsistency also would cause problems when it exists in simulators based on other methods and on other hydraulic variables such as equivalent freshwater head, or a quasi-stream function.

The inconsistency is most clearly demonstrated by consideration of hydrostatic conditions for a region of space in which pressure and concentration are approximated with a linear variation from the top to bottom of the region. If the pressure at the top of a region with height H is zero, then the bottom pressure, under hydrostatic conditions, is given by $p_B = \rho_{AVG}|g|H$, where ρ_{AVG} is the average density of fluid in the region. If linear relation (2) holds between density and concentration, then when the concentration varies linearly from top to bottom, the density does as well. If the density changes linearly, the pressure must change quadratically in order to maintain hydrostatic equilibrium. However, the approximation for pressure allows only a linear change across the region and a truly linear pressure change exists only under conditions of constant fluid density. Combining a linear change in density with a linear change in pressure in relation (15) would result in an upward velocity calculated at points in the upper half of the region and a downward velocity in the lower half. A zero velocity exists at the region centroid, however, as the density and pressure gradient are consistent at this point. The artificial velocities calculated within a region of space because of inconsistent approximation of pressure gradient and density would disperse a sharp transition zone even under hydrostatic conditions. Only employing ρ_{AVG} at all points in the region, in lieu of $\rho(C)$, would yield a calculated value of zero vertical velocity throughout.

As a result of this inconsistency, artificial velocities on the order of hundreds of meters per year may easily arise in simulation of common field situations. In the particular case where the transition zone is narrow, artificial velocities may have a significant effect on the transport solution. This is especially true for long-term or steady state simulations in which very small velocities strongly impact the solution. Using the convention of isoparametric coordinates (ξ, η) defined in Appendix B, the magnitude of artificial velocity in a finite element may be calculated at a Gauss point ($\xi = \eta = \mp 0.577$, as defined in Appendix A). The value is $v = 0.2885(k|g|\Delta\rho/\varepsilon\mu)$ or $v \sim 2830\ (k\Delta\rho/\varepsilon)$m/s, where $\Delta\rho$ is the difference in density from top to bottom of the element. For example, when permeability corresponds to that of silty sand, $k = 10^{-11}$ m^2 with porosity $\varepsilon = 0.1$, and fluid in an element changes from freshwater at the top to seawater at the bottom ($\Delta\rho = 25$ kg/m^3), the artificial velocity is about 220 m/yr. In simulating such a system with an inconsistent method, a sharp transition zone initially contained in one element could artificially begin to broaden at a rate of 440 m/yr, when no other natural velocities were superimposed on the system. Moreover, the velocity-dependent dispersion coefficients, relations (7)–(12), take on large values based on the artificial velocities and could disperse the sharp transition zone. This is clearly unacceptable for steady state simulation, and, depending on the geometry and scale of the system, could cause serious errors in simulations lasting a month or more.

Two examples of the effects of inconsistent velocity approximations on simulation results are offered in this paper. One example of a regional aquifer cross section in southern Oahu, Hawaii, is discussed later. The other example, discussed here,

relates to local scale simulation of saltwater upconing beneath a pumping well. *Reilly and Goodman* [1987] compared sharp interface and dispersed interface methods for analysis of the upconing problem. Their "comparison one" relates sharp and dispersed steady state interface results for a problem of radially symmetric upconing in a homogeneous, anisotropic aquifer cross section with steady pumpage from a partially penetrating well. The sharp interface solution used is that of *Bennett et al.* [1968, case C-5] from electrical analog analysis. The solution with dispersion was obtained using the SUTRA model [*Voss*, 1984]. Results from a version of SUTRA with inconsistent velocity approximations are compared here with those of *Reilly and Goodman* [1987] using the consistent approximations.

A 20-m long partially penetrating well centered 15 m below the aquifer top (Figure 1) pumps out 56 kg/s of water. Recharge is distributed along the top of the section (1.78×10^{-5} kg s^{-1} m^{-2}) and also occurs along the outside radial boundary. Along this vertical boundary, a constant hydrostatic pressure distribution is specified corresponding to freshwater above salt water with a 16-m-thick transition zone centered 20 m above the aquifer bottom. Along the bottom, a constant pressure corresponding to that at the bottom of the outer radial boundary is specified. No flow occurs across the axial boundary. Significant system parameters are as follows:

$$k_h = 2.56 \times 10^{-11}\text{m}^2$$

$$k_v = 1.00 \times 10^{-11}\text{m}^2$$

$$\varepsilon = 0.20$$

$$\rho_0 = 1000\ \text{kg/m}^3$$

$$\rho_{\text{saltwater}} = 1024.99\ \text{kg/m}^3$$

$$\alpha_L = 1.0\ \text{m}$$

$$\alpha_T = 0.5\ \text{m}$$

where k_h and k_v are horizontal and vertical permeabilities. Vertical discretization in the finite element mesh (930 nodes, 870 elements) is 4.0 m. Horizontal discretization increases from a spacing of 0.4 m to a constant spacing of 50 m past a radius of 100 m. The well radius is 0.35 m.

The steady state concentration distributions for the upconing problem with consistent and inconsistent velocity approximations are shown in Figure 2. The inconsistent velocity approximation widens the transition zone somewhat and causes a spatial instability in the numerical solution. Thus use of the inconsistent velocity approximation may lead to incorrect analysis of such a problem.

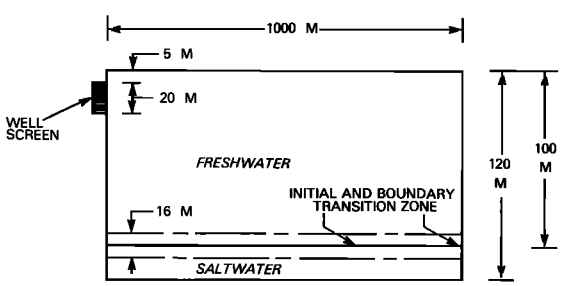

Fig. 1. Geometry of saltwater upconing simulation (adapted from *Reilly and Goodman* [1987]) (not to scale).

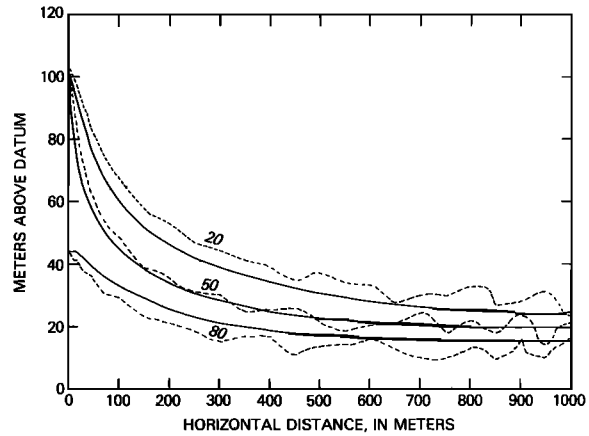

Fig. 2. Comparison of saltwater upconing simulations at steady state. Solid curve, consistent velocity approximation [from *Reilly and Goodman*, 1987]; dashed curve, inconsistent velocity approximation. Concentrations are given as percent saltwater.

An artificial velocity would be calculated in any numerical method whenever the functional approximation in space of pressure gradient and density are not consistent. A discrepancy would arise both in the velocity term of the fluid mass balance (equation (4)) and in evaluation of fluid velocity for transport; moreover, the discrepancy would generate artificial velocity-dependent dispersion coefficients (11) and (12). If density is allowed to vary spatially in the vertical direction as an Nth power polynomial, then pressure must be allowed to vary as an $N + 1$th power polynomial in order that the pressure gradient be consistent with density and vary to the Nth power. For finite elements and a linear density-concentration relationship, this would be satisfied by a choice of linear basis function discretization for concentration and quadratic basis function discretization for pressure. Quadratic basis functions, however, significantly increase computational expense and another approach may be preferable.

A consistent method has been developed by *Frind* [1982*a*] in a relatively economical finite element model that restricts the mesh to simple rectangular linear elements with one set of parallel sides aligned with both the gravity direction and the principal permeability directions. Consistency under these conditions is obtained by choosing to assign only one velocity per element. This value is calculated at the element centroid based on the average density for the element. Further, the term in the mass balance derived from the density-gravity term of Darcy's law is approximated using an average concentration for each element which again gives an average density for the entire element. While consistency is indeed obtained in this way, the order of approximation in the horizontal direction of density and velocity is also decreased. This may be a significant limitation in horizontally long elements as described below.

A desirable mesh design for cross-sectional simulation of regional fresh-water-saltwater aquifer systems often requires finer discretization in the vertical direction than in the horizontal direction. In order to adequately discretize concentrations in horizontally trending transition zones between freshwater and saltwater in a regional system, more nodes are usually required in the vertical direction than in the horizontal. This is true even when the aquifer is, for example, 10 km wide and only 100 m thick. Thus to maintain computational economy, elements with high aspect ratios (e.g., 1000 m wide

and 1 m high) must often be employed in such regional analysis. Numerical tests of a centroid-only velocity consistent method, similar to that of *Frind* [1982*a*], show that horizontal element-to-element oscillations in velocity can occur in meshes with large element aspect ratios. The oscillations are characterized by a velocity which points upward in one column of elements and downward in the next, giving rise to significant errors in concentration. The instability is exacerbated in regional simulations where the transition zone between fresh and saltwater is only few elements wide in the vertical direction. While this behavior may be managed or even eliminated by use of a fine horizontal discretization, some of the advantage of the economical finite element approach that uses one density value per element would be lost by requiring the use of both fine vertical and horizontal discretization on regional scale problems.

The restriction requiring fine horizontal discretization may, however, be circumvented in a consistent method. The requirement of consistency governs the choice of approximations only in the coordinate direction parallel to the direction of gravity. In other directions the density-gravity term drops out of both the fluid mass balance (equation (4)) and the velocity calculation based on (3). Thus within a region of space or finite element, a higher-order approximation for density may be employed horizontally rather than vertically.

The implementation of vertical-only consistency is best demonstrated for finite elements on a rectangular element with two sides aligned with the gravity direction. The approach would be to first calculate a density which varies bilinearly within an element according to $C(x, z, t)$ and (2) and then to decrease its variability only in the direction of gravity by averaging the density values vertically in the element. The averaged density in an element varies linearly transverse to the gravity direction and is constant along the gravity direction. The vertical velocity based on this density would vary linearly transverse to the direction of gravity and would be constant in the element along the direction of gravity. Horizontal velocities would be unaffected by the density averaging. Such an approximation gives a higher-order functional representation for the velocity field in a finite element mesh than does allowing just one velocity (and one density) value per element.

In the most general case of a bilinear quadrilateral finite element oriented arbitrarily to the gravity vector, the nature of a consistent approximation is necessarily more complex. One complexity results from the variability of density in two dimensions within each element. A second complexity results because the gravity vector is not necessarily parallel to any sides of a given finite element. In the local coordinate system within an element (defined in Appendix B), the gravity vector may change in both magnitude and direction from point to point, although it is invariant in global coordinates. A general finite element method may be developed by beginning with the assumption that if the numerical pressure gradient and density-gravity terms are consistently approximated in the local coordinate system in which basis functions are defined, then the terms will remain consistent after transformation to the global coordinate system. Thus consistency must be enforced separately in local coordinates for each vector component of the density gravity term. A general finite element method described by *Voss* [1984] is given in Appendix B and is implemented in the SUTRA model [*Voss*, 1984]. The consistent method has been verified on both regular rectangular finite element meshes and on irregular meshes containing nonrectangular finite elements. This is a significant modification to standard Galerkin finite element methodology that results in a consistent velocity approximation.

VERIFICATION OF VARIABLE DENSITY MODELS

The second component of a successful approach to simulation of variable density fluid movement is verification that a code accurately and stably represents the physics implied by the set of governing equations. In order to simulate narrow transition zones between freshwater and saltwater, verification of a consistent velocity approximation must be obtained. In particular, a simulator must accurately represent bulk flows driven by the buoyancy forces that arise in variable density fluids. The discussion below considers the popular "Henry problem" [*Henry*, 1964] verification, presents two test problems to verify consistency, and presents the "Elder problem" [*Elder*, 1967] for verification of purely bouyancy-driven flows.

Varible density transport models are typically verified by comparison with the *Henry* [1964] approximate analytic solution for steady state saltwater intrusion. However, no model to date has successfully matched the Henry solution, and the test is not, in general, a sufficient verification for variable density transport models. The Henry problem involves freshwater in a confined aquifer discharging to a vertical open sea boundary over a diffuse wedge of saltwater that has intruded the aquifer. A number of numerical models based on significantly different methods give nearly identical results for the Henry problem. These include a particle tracking model by *Pinder and Cooper* [1970], finite element models by *Segol et al.* [1975], *Huyakorn and Taylor* [1976], *Desai and Contractor* [1977], and *Frind* [1982*a*], a finite difference model by *INTERA* [1979], and the U.S. Geological Survey finite element model SUTRA [*Voss*, 1984]. None of these results match Henry's analytic solution. This may indicate some inaccuracy in Henry's results, possibly due to missing higher-order terms which were originally dropped for the sake of reducing computation time. While verification of a model by exact comparison with Henry's results is thus not presently possible, some confidence in the accuracy of a particular model for problems with highly dispersed transition zones may be gained if it matches the results of the above-listed suite of models.

Results of the SUTRA model are compared with results of other authors for the Henry problem. Figure 3 describes the

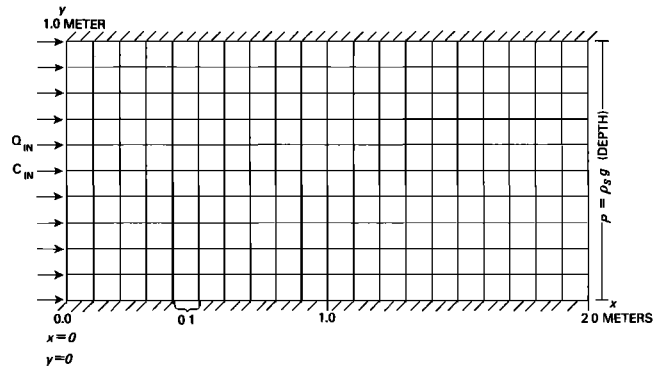

Fig. 3. Boundary conditions and SUTRA finite element mesh for *Henry* [1964] solution.

physical system and finite element mesh (231 nodes, 200 elements) employed by the SUTRA simulation. Velocity-dependent dispersion was neglected by *Henry* [1964] in favor of a constant dispersion coefficient in order to make a semi-analytic solution tractable. Dispersion is modelled in the numerical simulations by using a large constant value of molecular diffusivity and zero dispersivity.

The comparison between various models and the Henry solution [*Henry*, 1964] must be considered in different groups as the various authors have published either a different representation of the solution or have used different parameter values. Following most authors, the parameters chosen to match Henry's dimensionless values are

$$\varepsilon = 0.35$$

$$C_s = 0.0357 \left[\frac{\text{kg(dissolved solids)}}{\text{kg(seawater)}}\right]$$

$$\rho_s = 1024.99 \text{ kg/m}^3$$

$$= \text{seawater density}$$

$$\frac{\partial \rho}{\partial C} = 700 \left[\frac{\text{kg(seawater)}^2}{\text{(kg (dissolved solids) m}^3\text{)}}\right]$$

$$\rho_0 = 1000 \text{ kg/m}^3$$

$$Q_{IN} = 6.6 \times 10^{-2} \text{ kg/s}$$

$$k = 1.020408 \times 10^{-9} \text{ m}^2 \text{ (based on K} = 1.0 \times 10^{-2} \text{ m/s)}$$

$$|g| = 9.8 \text{ m/s}^2$$

$$\alpha_L = \alpha_T = 0.0$$

$$B = 1.0 \text{ m}$$

$$D_m = 6.6 \times 10^{-6} \text{ m}^2/\text{s}$$

$$D_m = 18.8571 \times 10^{-6} \text{ m}^2/\text{s} \qquad \text{two cases}$$

$$C_{IN} = 0.0$$

The total freshwater recharge is chosen as 6.6×10^{-5} m/s per meter of cross-section thickness (perpendicular to plane of section). Two different values of a total dispersion coefficient appear to have been used by the various authors. For the chosen total recharge rate and *Henry*'s [1964] nondimensional factor of total dispersion coefficient divided by recharge equal to 0.1 the total dispersion coefficient must be 6.6×10^{-6} m^2/s. Because the total dispersion coefficient for the SUTRA model (defined as the sum of molecular diffusion and mechanical dispersion in equation (1)) in the case of no velocity-dependent dispersion, is given by a product of porosity and the molecular diffusion coefficient, the diffusion coefficient should be set to 18.8571×10^{-6} m^2/s when the porosity is 0.35. This gives a simulated result for the concentration at the bottom of the aquifer after 100 min as shown in Figure 4, where a comparison is made with steady state results from three different models of *Huyakorn and Taylor* [1976]. Tests of longer simulations with the SUTRA model show that concentrations do not change appreciably after 100 min. Thus the curves are in excellent agreement.

The same parameters give a concentration distribution in space as shown in Figure 5. Here, the *Henry* [1964] solution for the 0.5 isochlor is compared with results of *Segol et al.* [1975] and results from new simulations using SUTRA and the *INTERA* [1979] transport code. Mesh blocks were 0.1 m

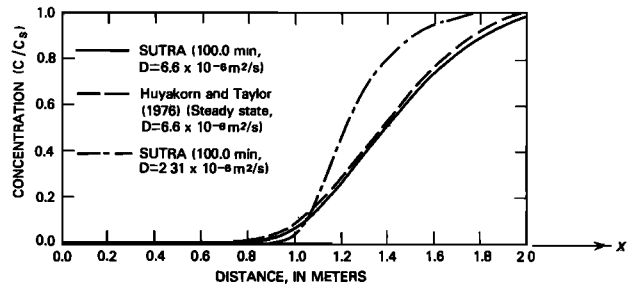

Fig. 4. Match of isochlors along bottom of aquifer for numerical results of *Huyakorn and Taylor* [1976] and SUTRA.

by 0.1 m for both the SUTRA finite element solution and INTERA solution. INTERA simulation was done with centered in time and centered in space finite difference approximations. SUTRA and INTERA results are nearly identical but do not compare well with Segol et al. and Henry. Moreover, the SUTRA results do not approach the Henry solution even for simulations lasting thousands of minutes.

Assigning a value of 6.6×10^{-6} m^2/s to the molecular diffusion coefficient would give a total dispersion coefficient of 2.31×10^{-6} m^2/s when the porosity is 0.35. This dispersion value, rather than that which Henry used appears to have been employed by *Pinder and Cooper* [1970], *Segol et al.* [1975], *Desai and Contractor* [1977], and *Frind* [1982*a*]. The discrepancy seems to have begun in the work by *Pinder and Cooper* [1970], who used a form of the solute mass balance equation divided by porosity, whereas in his semianalytical solution, *Henry* [1964] did not divide by porosity. Published results for these models and SUTRA using the molecular diffusion value 6.6×10^{-6} m^2/s are compared to the Henry solution in Figure 6. Simulated results are nearly identical including those of *Desai and Contractor* [1977] who employed a coarser mesh than the others. Because a total dispersion value other than Henry's were used, these solutions should not and do not compare with Henry's; however, the solutions using Henry's total dispersion of Figure 5 are an even poorer match with those of Henry.

Steady conditions in saltwater intrusion problems are approached rather slowly; therefore *Pinder and Cooper* [1970] suggested that the solution would converge to *Henry*'s [1964] from opposite sides when different initial conditions are used for the problem. Figure 7 confirms for the case of total dispersion coefficient equal to 2.31×10^{-6} m^2/s that the same solu-

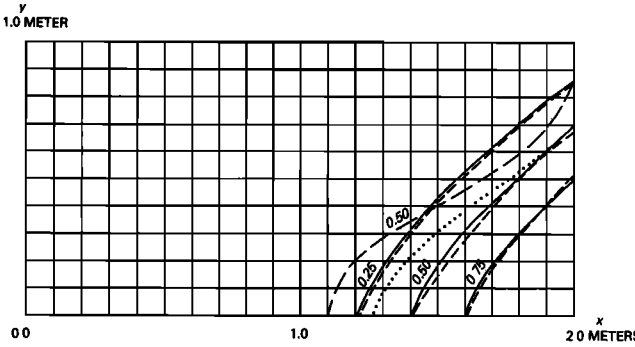

Fig. 5. Match of isochlor contours for *Henry* [1964] analytical solution (for 0.50 isochlor) (long-dashed curves); INTERA code solution (short-dashed curves); *Segol et al.* [1975] (dotted curve); and SUTRA solution for (0.25, 0.50, 0.75) isochlors (solid curves).

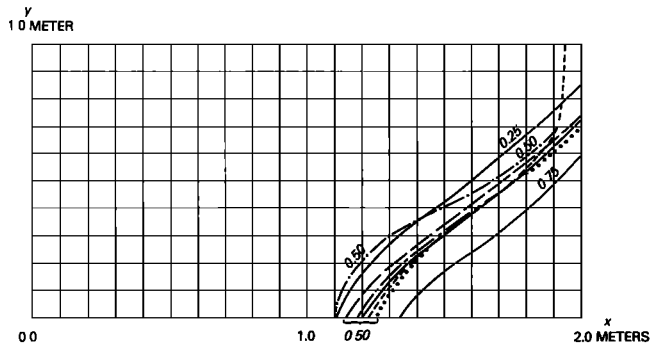

Fig. 6. Match of 0.50 isochlor contours for *Henry* [1964] problem with simulated results for $D_m = 6.6 \times 10^{-6}$ m^2/s of *Pinder and Cooper* [1970] (short-dashed curve); *Segol et al.* [1975] (dotted curve); *Frind* [1982] (long- and short-dashed curve); and *Desai and Contractor* [1977] (long-dashed curve). SUTRA results at isochlors (0.25, 0.50, 0.75) (solid curve). *Henry* [1964] solution for $D_m = 18.8571 \times 10^{-6}$ m^2/s (0.50 isochlor, dashed-dotted curve).

tion is approached by the SUTRA model from both sides; however, this solution is again not Henry's. The initial condition for the curve approaching from the left is an aquifer filled with saltwater; curves from the right begin with an aquifer filled with freshwater.

Through the preponderance of simulators that have closely matched results for the Pinder-Cooper version of the Henry problem [*Henry*, 1964] this has become a standard test for all variable density transport models. However, because of the unrealistically large amount of dispersion introduced in the solution by the constant total dispersion coefficient, this test does not check whether a model is consistent or whether it accurately represents density driven flows, nor does it check whether a model can represent field situations with relatively narrow transition zones. In fact, Henry problem results are the same for both inconsistent and consistent approximations. Thus when the transition zone is broadly dispersed and concentration gradients are low, the artificial velocities created by the inconsistent approach are insignificant compared with the field velocities, and the artificial components of the velocity-dependent dispersion are small relative to the total dispersion. The Henry problem is thus a verification of a variable-density transport model only for simulation of highly dispersed transition zones.

Two additional tests are suggested to check for consistency: first, steady state simulation of a completely closed horizontal aquifer containing a horizontal layer of freshwater above a layer of saltwater; and second, steady state simulation of the same system with open vertical sides and uniform horizontal flow. The first additional test simply checks for consistency under hydrostatic conditions with a stable density configuration and no flow allowed across any boundaries. The choice of geometric scale and hydraulic parameters is not important because the system goes to steady state. Longitudinal and transverse dispersivities should be set to values equivalent to the length of the largest finite element, and diffusivity should be set to zero. The correct solution is obtained only if the pressure gradient and density-gravity terms are consistently approximated. In the correct solution, the transition zone should remain fixed in one row of elements. The second additional test checks for consistency in a system where flow is parallel to the transition zone and the mesh. The simulation should be carried out with a longitudinal dispersivity of half the horizontal mesh spacing and a zero transverse dispersivity and diffusivity. The flow may be set up by creating a horizontal pressure difference between the hydrostatic pressure conditions that are specified along the vertical slides. The correct steady state solution maintains the transition zone in the same single row of elements. Inconsistent approximations result in spreading of the sharp interface in both cases.

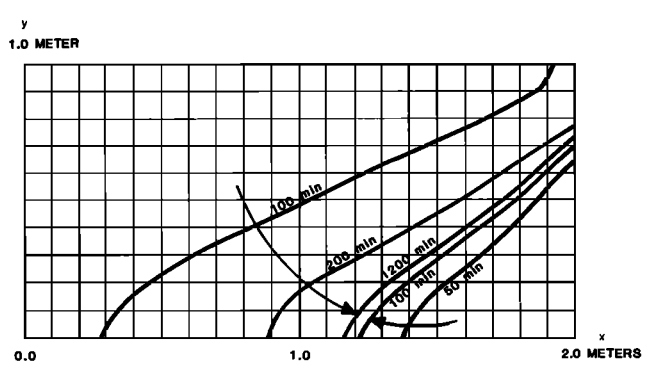

Fig. 7. Approach to solution from initially fresh and initially salty conditions for *Henry* [1964] problem using SUTRA.

The numerical results of *Elder* [1967] for a problem of complex natural convection are further suggested as a basis for verification of transport simulators. The primary value of this test is to verify the accuracy of a simulator in representing bulk fluid flow driven purely by fluid density differences. Elder dealt with thermally driven convection in a cross-section. The solute analog to his "short-heater problem" is a closed rectangular box, modeled in cross section, with a source of solute at the top implemented as a specified concentration boundary condition with a value of one (Figure 8) and concentration specified with a value of zero along the entire base. A zero value of pressure is specified at each upper corner, and the pressure is initially hydrostatic. Solute enters the initially pure water by diffusion, increases its density, and thereby begins a circulation process. The following data is used to match Elder's dimensionless results:

$$\varepsilon = 0.1$$

$$k = 4.845 \times 10^{-13} \text{ m}^2$$

$$\mu = 1.0 \times 10^{-3} \text{ kg m}^{-1} \text{ s}^{-1}$$

$$C_{\text{initial}} = 0$$

$$\rho = 1000 \text{ kg/m}^3 + (200)C$$

$$|g| = 9.81 \text{ m/s}^2$$

$$D_m = 3.565 \times 10^{-6} \text{ m}^2/\text{s}$$

$$\alpha_L = \alpha_T = 0$$

Note that $\rho_{\max}(C = C_{\max}) = \rho(C = 1) = 1200$ kg/m^3.

Elder [1967] employed a standard finite difference representation of the governing equations for vorticity, stream function, and thermal energy balance. The equations were solved sequentially with a forward temporal difference. The matrix equations were solved sequentially with a forward temporal difference. The matrix equations were resolved iteratively and an overrelaxed alternating direction method [*Elder*, 1966] was used for the vorticity equation. Elder's grid consists of 80 nodes laterally and 40 nodes vertically, and time discretization

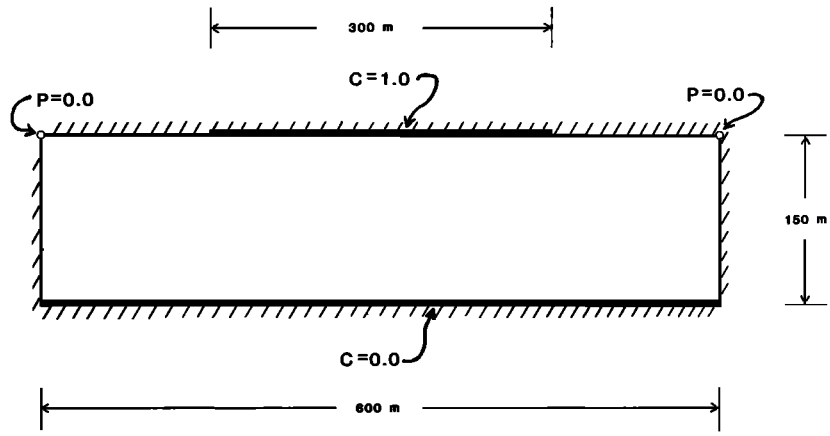

Fig. 8. Boundary conditions for *Elder* [1967] problem.

was such that it took 20 steps to reach the first point of comparison (1 year elapsed time) discussed below.

The problem is simulated with the SUTRA model, using a mesh coarser than *Elder*'s [1967], consisting of 44 finite elements horizontally and 25 elements vertically (1170 nodes and 1100 elements). The simulation is carried out with time steps of 1 month (2.6298×10^6 s), and iterations for each time step are considered complete when the maximum absolute change for all nodes from the previous iteration falls below 500 Pa for pressure and 0.01 for concentration. While the simulation could theoretically be carried out on only the left or right half of the system, modeling the entire box checks the ability of the simulator to produce symmetric vortices.

Figure 9*a* compares nondimensional concentration results of simulation with SUTRA to nondimensional temperature results of *Elder* [1967]. Figure 9*b* compares the flow field simulated by SUTRA with the steamline results of *Elder* [1967]. The concentration field is strongly coupled to the complex flow field which evolves through a series of transient anticlockwise and clockwise vortices. Although SUTRA uses somewhat coarser spatial and temporal discretization, the results compare very well, spatially and through time, showing that both numerical solutions give similar representation of the complex density-driven flows and solute transport behavior. As with the Henry problem, comparison of results of a given simulator with other numerical solutions lends confidence in the accuracy of the simulator.

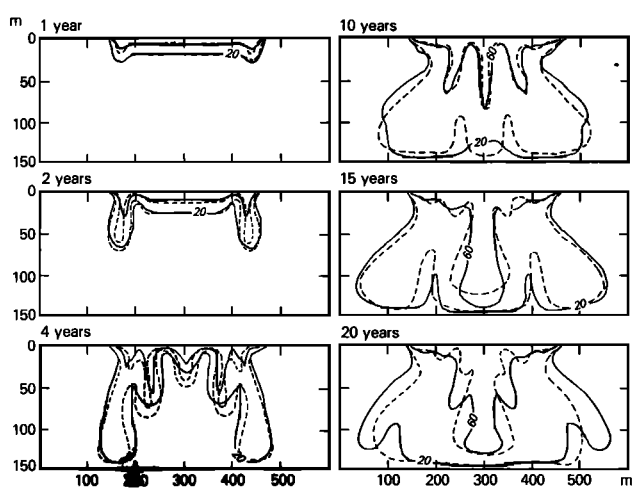

Fig. 9*a*. Comparison of nondimensional results for *Elder* [1967] problem, showing 20 and 60% of maximum concentrations for SUTRA (solid curves) and of maximum temperature from Elder (dashed currves).

Practical Discretization for Narrow Transition Zones

The third component of a successful approach to obtaining accurate and stable simulations of variable density transport problems is the careful choice of spatial and temporal discretization. Spatial discretization is sufficient if it (1) adequately describes spatial variations in aquifer parameters and represents flow and transport processes and (2) provides numerical stability. Relatively fine discretization must often be used in directions both along flow lines and across flow lines. A desirable mesh design often employs elements that are much longer horizontally than vertically, as is discussed in a previous section. Practical mesh design is a somewhat qualitative subject and appropriate choice of element size is discussed in the following.

Along flow lines a mesh Peclet number Pe_m, which varies from point to point, may be defined depending on local mesh size, fluid velocity, and dispersion coefficients. The mesh Peclet number is given as

$$Pe_m = \frac{|v|\Delta_s L}{D_L} = \frac{|v|\Delta_s L}{(D_m + \alpha_L |v|)} \tag{16}$$

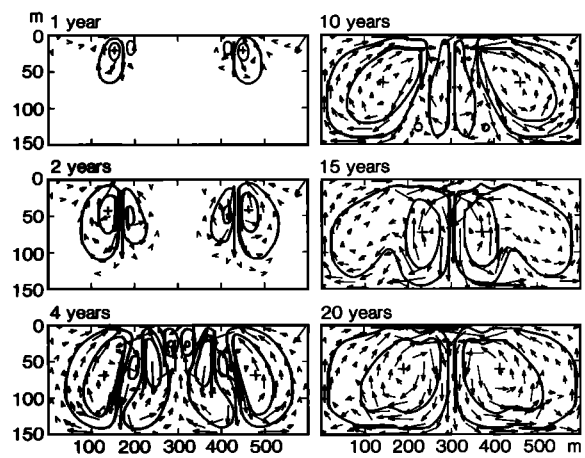

Fig. 9*b*. Comparison of flow fields for *Elder* [1967] problem, showing every seventh element centroid velocity for SUTRA and steamlines given by Elder.

where $\Delta_s L$ is the local distance between sides of an element measured along the local flow direction, $|v|$ is the magnitude of local velocity; and D_L is the total longitudinal dispersion coefficient as defined in (16). This Peclet number is a measure of the amount of local advective transport relative to the local amount of diffusive and dispersive transport. When, as in most field cases, molecular diffusion D_m is small relative to mechanical dispersion, $D_L \approx \alpha_L|v|$, and the mesh Peclet number is

$$Pe_m \approx \left(\frac{\Delta_s L}{\alpha_L}\right) \tag{17}$$

When the mesh Peclet number is high, centered finite difference and Galerkin finite element approximations can give values of concentration which oscillate in space. For the numerical method described here, oscillations do not occur when the mesh Peclet number is approximately four or less ($Pe_m < 4$). Thus in designing a mesh, discretization must be chosen so that along the direction of flow, $4\alpha_L > \Delta_s L$. Should this requirement be satisfied everywhere in a mesh except in small localized regions, the solution will likely oscillate only in these regions and may not spoil the rest of the solution, resulting in an acceptable solution to the problem. If oversized elements are used where longitudinal concentration gradients are low, oscillations may not occur at all and the criterion may be safely violated by more than an order of magnitude. This economy is often possible in cross-sectional analysis of seawater intrusion in aquifers, as is shown in the Hawaii example that follows.

In the direction perpendicular to flow lines, only dispersive transport takes place. Thus spatial discretization in the direction perpendicular to flow lines must be sufficient to represent a solution to the equation describing a diffusive process in that direction. The total transverse dispersion coefficient D_T is made up of a molecular diffusion component and a mechanical dispersion component, $D_T = (D_m + \alpha_T|v|)$. In the steady transport case where D_T is zero, with any finite value of total longitudinal dispersion coefficient D_L the analytical solution gives constant concentration along each streamline. In particular, for freshwater and saltwater under these conditions, the fluids do not mix at all and are separated by a perfectly sharp interface. In the simulation of these conditions with $Pe_m < 4$ and a flow field not parallel to the sides of a mesh composed of regular rectangular elements, the numerical solution gives a transition zone with a thickness of a few elements. Thus the sharp analytical solution for zero α_T is not possible to obtain numerically as transverse discretization is never fine enough to represent the sharp interface solution. This error disappears as $\Delta_s T/D_T$ decreases, where $\Delta_s T$ is the transverse spacing. *Frind* [1982*c*] has suggested alleviating this problem through mesh orientation that parallels streamlines.

In order to determine the amount of transverse dispersion caused by discretization, a steady state transport simulation for any given problem may be run with $\alpha_T = 0$ to obtain the narrowest transition zone possible with a given flow field and given mesh. A rule of thumb for accurate transverse discretization in cases with velocity-dependent dispersion is to choose the mesh spacing such that $\Delta_s T \lesssim \alpha_T$, although numerical experiments show that $\Delta_s T \lesssim 10\ \alpha_T$ may be adequate for many situations. This stringent criterion has been violated in most published transport simulations, calling into question the validity of simulation-fitted values of transverse dispersivity. For a mesh that is coarse in the direction transverse to flow, the numerical solution is quite insensitive to the value of transverse dispersivity, α_T. The true effect of a low value of α_T is almost always lost in the artificial dispersion caused by large transverse mesh spacing.

Choice of discretization in time, following a change in stress on a system, should give early time solutions a small time step and late time solutions a larger time step. Time steps for density-dependent transport simulation must be small when beginning a simulation from poor initial conditions with sharp concentration gradients. A small time step for the transport solution may be defined as that which would allow a particle of fluid to traverse on the order of a tenth of the distance across any element. A large time step at early time would allow fluid to traverse on the order of one element per step. Restrictions on time step size for stability of transport solutions are most likely to be found in mesh areas of converging flow, such as near wells. This is because velocities are high and mesh sizes likely small in those areas. At late time, when concentration gradients tend to be less sharp, much larger time steps may be taken without sacrificing either numerical accuracy or stability.

EXAMPLE: SOUTHERN OAHU, HAWAII

Simulation of groundwater flow and movement of dissolved solids in the southern Oahu aquifer near Honolulu, Hawaii, is a difficult problem, as the transition between freshwater and saltwater is narrow inland, although it is broad near the coast. Because important hydraulic boundaries are relatively close to areas of interest near pumping centers, the entire aquifer must be simulated, including both narrow and broad portions of the transition zone. The SUTRA model [*Voss*, 1984] is applied to the southern Oahu system on a well-discretized but practical mesh in order to demonstrate the efficacy of the suggested modeling approach. Comprehensive description of hydrologic modeling of the southern Oahu aquifer is given by *Souza and Voss* [1987]. In this section, a consistent velocity approximation is demonstrated to be a vital factor in successful simulation of the southern Oahu aquifer.

The southern Oahu basaltic aquifer is composed of thinly bedded lava and rubble layers (thicknesses from 1 to 10 m) on the southwest flank of the Koolau range. Regionally, the aquifer is very thick ($\sim$1800 m) and quite permeable ($K \sim 500$ m/day). The aquifer fabric may be expected to have vertically anisotropic permeability between 10:1 and 10000:1 due to the layered structure, although the regional anisotropy value has not been established in previous studies. The basalt dips down toward the southwest at an angle of a few degrees. Near the coast and below Pearl Harbor (the involuted inland water body of Figure 10), the basalt is semiconfined by a wedge of interlaced sediment and coral formations, referred to as the "caprock" (Figure 11).

Primary recharge occurs over the Koolau mountains where significant intrusions of vertical dike walls into the horizontal beds make horizontal flow difficult. The dike-intruded region is considered a no-flow boundary for the sake of the aquifer model that contributes a large specified recharge to the basalt aquifer due to spills over and around dike walls. A general description of hydrogeology is given in the work by *Visher and Mink* [1964].

Discharge in the undeveloped state of the aquifer occurs primarily at springs along the inland edge of the caprock. Some diffused discharge is expected as upwards leakage

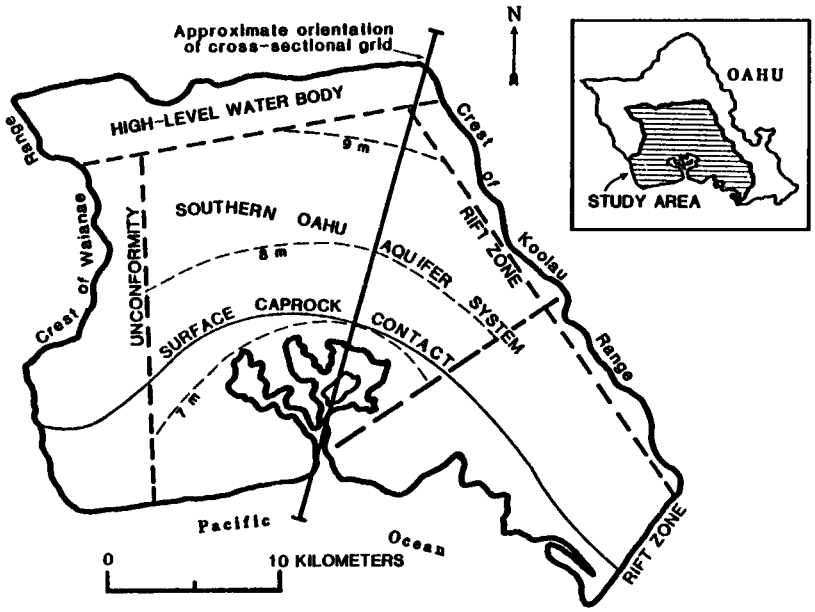

Fig. 10. Southern Oahu aquifer map with boundaries and 1958 hydraulic heads adapted from *Mink* [1980].

through the caprock into Pearl Harbor. Total throughflow in the aquifer is on the order of 10^6 m^3/day (255 Mgal/day) [*Mink*, 1980].

A cross-sectional model is highly appropriate for representation of system behavior because of the regionwide nearly uniform flow field in which lateral convergence is negligible. Moreover, pumping is spread in a narrow band approximately parallel to both contours of equal hydraulic head and to the surface-caprock contact near the edge of Pearl Harbor. Initial hydraulic head in the system (predevelopment, 1890) was 10–13 m, leading to a 400- to 520-m-thick freshwater zone above the seawater interface estimated from the equilibrium Ghyben-Herzberg principle. Present-day heads are lower as a result of significant pumping stress and range from 5 to 8 m. The present-day freshwater lens would be only 200 to 320 m thick if it were in static equilibrium with the sea. In fact, the interface is not sharp everywhere in the aquifer (Figure 11) and it is not clear whether static equilibrium exists under current pumping conditions. Thus a variable density model capable of simulating transient conditions is required to evaluate the system.

The simulated region includes the dike-free basalt aquifer and a portion of the caprock similar to that shown in Figure 11. The finite element mesh for the cross section (702 nodes, 646 elements) has a portion with very fine vertical discretization (15.24 m) in the region of the aquifer where the transition zone between freshwater and saltwater is expected to reside (Figure 12). This allows sufficient discretization to represent the thin part of the transition zone. Below this region, concentrations, velocities, and pressures change very slowly in space and coarse discretization is sufficient. Sharp pressure changes and converging high fluid velocities occur at the springs near the edge of the caprock; thus horizontal discretization is finest in this region (304.8 m). Although regional longitudinal dispersivity is expected to be less than 100 m, horizontal spacing may greatly exceed the stability limit of 400 m based on relation (17), because lines of constant concentration will, for the most part, parallel the flow directions. Here, on the regional scale under steady conditions, longitudinal transport is less significant than transverse transport in defining the concentration distribution in the transition zone.

All boundaries of the mesh are closed to flow except where (1) freshwater recharge from the dike zone is specified at the back of the aquifer, (2) pressure is specified to be zero below

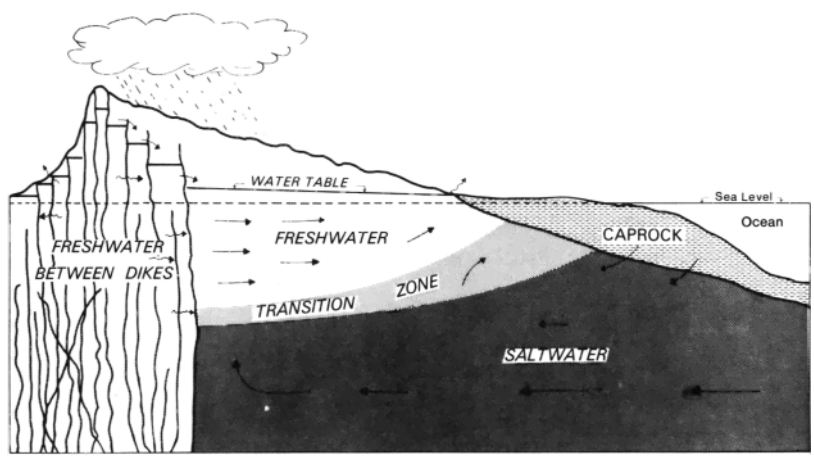

Fig. 11. Typical cross section of southern Oahu aquifers (not to scale).

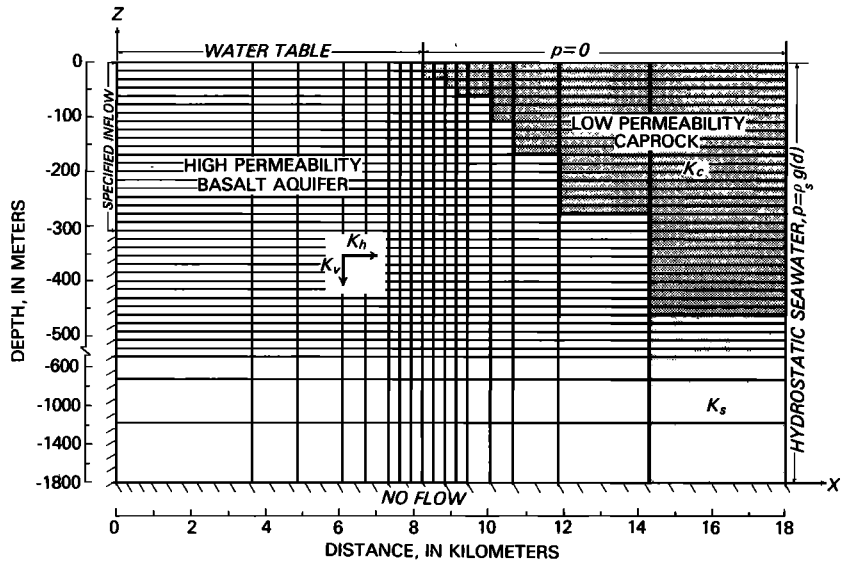

Fig. 12. Mesh for cross-sectional finite element model of southern Oahu aquifer (not to scale).

Pearl Harbor, and (3) pressure is specified to be hydrostatic, based on a column of seawater where the mesh is arbitrarily cut off on the seaward end. A higher impedance is specified along the seaward end below the caprock to represent the effect of the aquifer seaward of the boundary. A parsimonious model identification uses only six parameters to characterize the entire system behavior [*Souza and Voss*, 1987]. These values, as well as known system constants, define the 1-m-thick (in direction perpendicular to plane of section) representation of the system:

$$K_h = 457.2 \text{ m/day}$$

$$K_h/K_v = 200$$

$$K \text{ caprock} = K_h\, 10^{-4}$$

$$k_s = K_h\, 10^{-2}$$

$$S_y = \varepsilon = 0.04$$

$$\alpha = 2.5 \times 10^{-9} \text{ Pa}^{-1}$$

$$Q \text{ inflow} = 0.404 \text{ kg/s}$$

$$\rho_0 = 1000 \text{ kg/m}^3$$

$$\partial\rho/\partial C = 700 \text{ kg/m}^3$$

$$\beta = 4.47 \times 10^{-10} \text{ Pa}^{-1}$$

$$\mu = 1.0 \times 10^{-3} (\text{kg m}^{-1} \text{ s}^{-1})$$

$$\alpha_L = 80 \text{ m}$$

$$\alpha_T = 0.20 \text{ m}$$

$$C \text{ seawater} = 0.0357$$

$$\rho \text{ seawater} = 1024.99 \text{ kg/m}^3$$

where K_h and K_v are horizontal and vertical hydraulic conductivity, K_s is the hydraulic conductivity of the sea boundary, and C is the dissolved solids concentration as a mass fraction.

The simulated concentration distribution for predevelopment steady state conditions is shown in Figure 13 to scale and in Figure 14 with vertical exaggeration. The transition zone is very sharp inland, as expected, and gradually broadens near the caprock. The predevelopment velocity field (Figure 15) illustrates the saltwater circulation, including spring discharge near the caprock edge, and diffuse discharge through the caprock.

These solutions are impossible to obtain with an inconsistent velocity approximation (standard Galerkin method) as demonstrated by comparison in Figure 16 (for $K_h/K_v = 20$). Experiments show that neither low values of dispersivity nor high anisotropy (K_h/K_v) allow a relatively narrow transition zone to be simulated with the inconsistent approximation. The artificial velocity and resultant dispersion generated by the inconsistent approximation give highly incorrect results, overwhelming the physical dispersion in the system. However, accurate simulation based on a consistent velocity approximation provides a fundamental tool for hydrologic analysis of the system as described in the work by *Souza and Voss* [1987].

Discussion

Analysis of a freshwater-saltwater aquifer system that contains a relatively narrow transition zone is a difficult problem for variable density transport simulation. However, such analysis is desirable as narrow transition zones are often encountered in the field. Most published analyses either deal directly with the case where data indicates a broad transition zone, or give simulation results that show a broad zone. Based on the typical difficulties expected in modelling variable den-

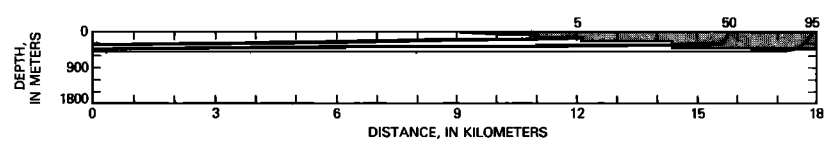

Fig. 13. Simulated predevelopment distribution of total dissolved solids (as percent seawater) for southern Oahu aquifer (to scale).

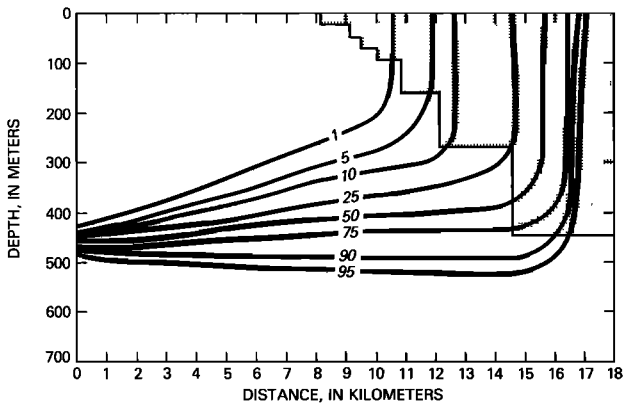

Fig. 14. Transition zone as simulated for predevelopment conditions (concentration as percent seawater) for southern Oahu aquifer (not to scale).

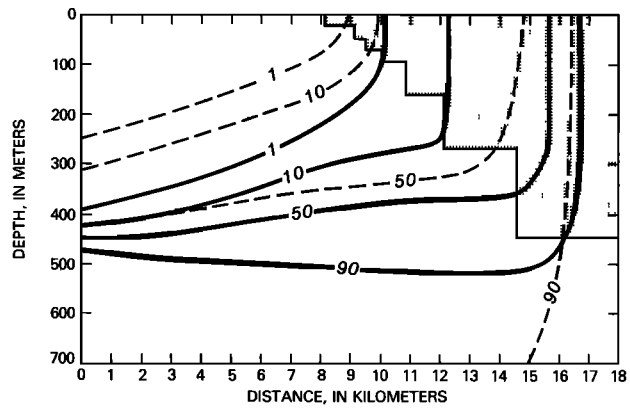

Fig. 16. Comparison of simulated predevelopment transition zone for Southern Oahu aquifer between model based on inconsistent (dashed curves) velocity discretization and consistent (solid curves) discretization (concentration as percent seawater) (not to scale).

sity transport, speculation may be warranted with regard to whether these analyses have accurately represented variable density transport as described by the standard governing equations. Errors in the simulation of the dynamics of a narrow transition zone stem from any inconsistencies, inaccuracies or instabilities inherent in a given model. The likely sources of simulation error are threefold. First, inconsistent approximations of terms involved in the fluid velocity calculation can lead to large artificial velocity and dispersion components. Second, inaccuracy can occur in representation of bulk fluid flows driven by density differences in the fluid. Tests typically used to verify variable density flow and solute transport models do not verify that a given model is free of the above sources of error. Third, discretization is typically too coarse for the desired level of transverse dispersion.

The following modeling approach alleviates these difficulties.

1. A consistent velocity approximation must be employed. The standard Galerkin finite element method gives an inconsistent velocity approximation that can generate artificial velocities and dispersion which overwhelm physical dispersion in a simulation. Finite difference methods may or may not be consistent, depending on the particular interpolations used. A modified general Galerkin finite element method (presented herein) gives a consistent velocity approximation for bilinear quadrilateral elements. The modified Galerkin method employs pressure gradient and density gravity approximating functions that are consistent in the local coordinate system of each element.

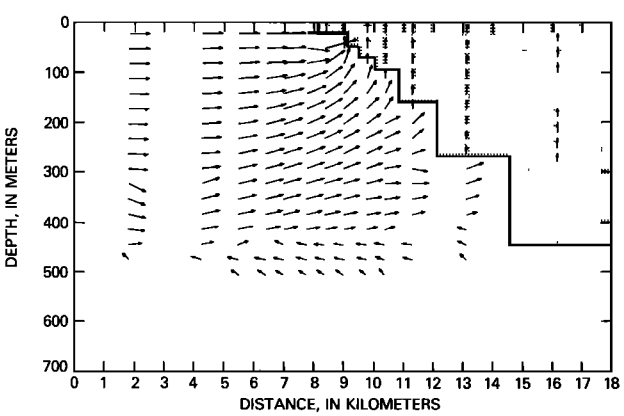

Fig. 15. Velocity field as simulated for predevelopment conditions in southern Oahu aquifer. (Angles are scaled to show true direction on exaggerated map.) Largest vector = 7.3×10^{-5} m/s at direction 7.5° above horizontal, occurs just below inland edge of caprock. Vector lengths are proportional to log of magnitude. Vectors less than 0.25% of maximum velocity are not plotted (not to scale).

2. Three tests in addition to the *Henry* [1964] seawater intrusion problem should be carried out to verify a simulator. The Henry problem serves only as a basis for verifying a variable density transport code in the case of highly dispersed transition zones. The test gives nearly identical results with inconsistent and consistent formulations; thus the inaccuracies of inconsistent simulators can not be detected. Further, the test only weakly verifies accuracy in simulating bulk flow driven by density differences. Two of the additional tests are simple checks for consistency of the velocity approximation. These simulate a system with a narrow transition that should remain narrow for all long-term and steady state simulations. The third additional test is the solute analog of the *Elder* [1967] natural convection problem. This verifies the accuracy of simulation of flow driven purely by density differences in the fluid.

3. Spatial and temporal discretization must be sufficient to guarantee accuracy and stability. In particular, vertical discretization should be on the order of the transverse dispersivity value when flow is predominantly horizontal. This requires unrealistically fine discretization in some cases which must be compromised. Thus transport simulation studies should always begin with a steady state simulation for the case of zero transverse dispersion. This checks for the narrowest transition zone possible with a given mesh and flow field.

The fine gridding required to obtain stable and accurate solutions when transition zones are narrow leads to expensive computer runs on field scale problems. While this is unfortunate, the expense of transport simulation is a natural and possibly unavoidable feature of the problem. Even numerical solutions by particle tracking or a method of characteristics, which do not have stringent stability restrictions for problems with high Peclet numbers, require fine discretization or a large number of tracking particles for accurate approximation of the dispersion term when the dispersivity is small but nonzero. Thus computational expense may be unavoidable because a large amount of information must be borne by any numerical method to simultaneously define both the concentration dis-

tribution within and movement of narrow finite thickness transition zones.

In order to guarantee useful results, a variable density flow and solute transport simulator must be based on a consistent velocity approximation, must be verified with the beforementioned tests, and must be used with proper spatial and temporal discretization. An illustrative application of such a simulator is the analysis of the regional aquifer of southern Oahu, Hawaii, that contains both narrow and broad sections of a freshwater-saltwater transition zone. Successful evaluation of the effects of newly proposed dispersion models in such a system would require analysis based on this modeling approach. Simulation based on this approach makes possible state-of-the-art analysis of a range of difficult problems at various scales.

APPENDIX A: WEIGHTED RESIDUAL METHOD

Applying a weighted residual method to the fluid mass balance, (4) results in NN relations:

$$\int_V \left[\rho S_{op} \frac{\partial p}{\partial t}\right]\phi_i \, dV + \int_V \left[\varepsilon \frac{\partial \rho}{\partial C}\frac{\partial C}{\partial t}\right]\phi_i \, dV + \int_V (\nabla \cdot \varepsilon\rho \mathbf{v})\phi_i \, dV = \int_V Q_p \phi_i \, dV \qquad i = \overline{1, NN} \tag{A1}$$

where V is volume. An integrated finite difference technique for the time derivative and source term may be implemented by assuming that the complete term involving the time derivative and the source has a constant value throughout a cell surrounding the node. The cell extends to the boundary defined by the connected bisectors of opposite sides of all elements contiguous to a node (Figure 17). The volume of the cell at node i, V_i, is given by

$$V_i = \int_V \phi_i \, dV \tag{A2}$$

By clearing the integrals of constants, applying Green's theorem to the term containing velocity, employing Darcy's law (equation (3)) and the general boundary condition (6), the weighted residual relation becomes

$$\left(\frac{S_y}{b|g|} + \rho S_{op}\right)_i V_i \frac{\partial p_i}{\partial t} + \left(\varepsilon \frac{\partial \rho}{\partial C}\right)_i V_i \frac{\partial C_i}{\partial t} + \int_V \left[\left(\frac{\mathbf{k}\rho}{\mu}\right) \cdot (\nabla p - \rho \mathbf{g})\right] \cdot \nabla \phi_i \, dV = Q_i + Q_{IN_i} \tag{A3}$$

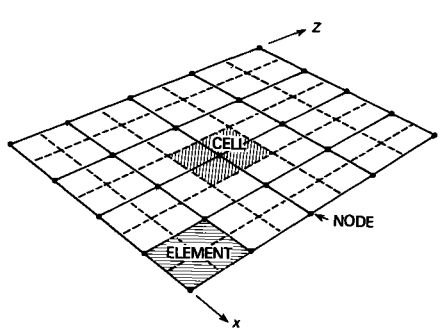

Fig. 17. Cells, elements, and nodes for a two-dimensional finite element mesh composed of quadrilateral elements.

in which the definition for fluid mass source $Q_i(x, z, t)$, M/T:

$$Q_p \equiv \sum_{i=1}^{NN} \left(\frac{Q_i}{V_i}\right) \tag{A4a}$$

has been employed and $Q_{IN_i}(x, z, t)$, M/T, is the fluid mass source at node i along the boundary Γ of the model region

$$Q_{IN}{}^* \equiv \sum_{i=1}^{NN} \left(\frac{Q_{IN_i}}{A_i}\right) \tag{A4b}$$

where A_i is the area of model boundary contained in cell i.

The general boundary condition employed in (A3) has the form

$$-\int_\Gamma (\varepsilon\rho \mathbf{v} \cdot \mathbf{n})\, \phi_i \, d\Gamma = \int_\Gamma Q_{IN}{}^* \phi_i \, d\Gamma + \int_\Gamma \left(\frac{S_y}{|g|}\frac{\partial p}{\partial t}\right)\phi_i \, d\Gamma \tag{A5a}$$

where $\mathbf{n}$ is the outward unit normal at the boundary and the last term has been evaluated as constant for each cell:

$$\int_\Gamma \left(\frac{S_y}{|g|}\frac{\partial p}{\partial t}\right)\phi_i \, d\Gamma = \left(\frac{S_y}{|g|}\frac{\partial p}{\partial t}\right)_i A_i = \left(\frac{S_y}{|g|}\frac{\partial p}{\partial t}\right)_i \frac{V_i}{b_i} \tag{A5b}$$

where $b_i(x, z)$ is effective cell height, $b_i = V_i/A_i$. In a horizontal rectangular element abutting the water table, b_i is half of the element height.

Discretization of the term involving permeability in (A3) using (13) gives

$$\int_V \left[\left(\frac{\mathbf{k}\rho}{\mu}\right) \cdot (\nabla p - \rho \mathbf{g})\right] \cdot \nabla \phi_i \, dV = \sum_{j=1}^{NN} p_j(t) \int_V \left[\left(\frac{\mathbf{k}\rho}{\mu}\right) \cdot \nabla \phi_j\right] \cdot \nabla \phi_i \, dV - \int_V \left[\left(\frac{\mathbf{k}\rho}{\mu}\right) \cdot (\rho \mathbf{g})\right] \cdot \nabla \phi_i \, dV \tag{A6}$$

Discretization of the $(\rho \mathbf{g})$ term is discussed in the consistent velocity section of the text and in Appendix B.

Discretizing the time derivatives using a backwards finite difference approximation

$$\frac{dp_i}{dt} = \frac{p_i{}^{n+1} - p_i{}^n}{\Delta t_{n+1}} \tag{A7}$$

$$\frac{dC_i}{dt} = \frac{C_i{}^n - C_i{}^{n-1}}{\Delta t_n} \tag{A8}$$

where

$$\Delta t_n = t_n - t_{n-1} \tag{A9}$$

$$p_i^n = p_i(t_n) \tag{A10}$$

$$C_i^n = C_i(t_n) \tag{A11}$$

and employing relation (A9) results in a form of (A3) which may be solved for pressure at all nodes, $p_i{}^{n+1}$. All coefficients except $(\partial C/\partial t)$ are evaluated by linear projection to the half time level $(n + \frac{1}{2})$ when only a single iteration is allowed per time step and at the $(n + 1)$ time level for time steps with multiple iterations. The $(\partial C/\partial t)$ term is usually small for seawater intrusion and thus is lagged one time step.

The integrations are carried out element by element after transforming the quadrilateral element to a local coordinate system in which each element is a square with sides of length two. The numerical Gauss integration uses two Gauss point

locations in each local coordinate direction (Figure 18). At each of the four Gauss points in an element, density is evaluated as a function of the bilinearly interpolated concentration $C(t_{n+1})$, at that point according to relation (2). At the nodes, density is evaluated based on the nodal concentration value $C_i(t_{n+1})$ from relation (2). In the term involving gravity, however, a special evaluation of the density values at Gauss points must be made in order to be consistent with the local pressure gradient, as is described in the main text and in Appendix B.

Verification of the water table form of the cross-sectional fluid mass balance was made by comparison of numerical solutions with the general solution of *Neuman* [1974]. Although fluid storage is accounted for at a moving water table by this formulation, the position of a water table is held fixed in space throughout a simulation. This is a practical approach as long as true movement of the water table is only a small fraction of the total height of the aquifer unit, as is discussed by *Neuman* [1974] in relation to analytic solution.

The weighted residual method applied to the solute mass balance (equation (1)) yields NN relations

$$\int_V \left(\varepsilon\rho \frac{\partial C}{\partial t}\right)\phi_i\, \delta V + \int_V (\varepsilon\rho \mathbf{v}\cdot\nabla C)\phi_i\, dV - \int_V \{\nabla\cdot[\varepsilon\rho(D_m\mathbf{I}+\mathbf{D})\cdot\nabla C]\}\phi_i\, dV = \int_V [Q_p(C^*-C)]\phi_i\, dV \qquad i=\overline{1, NN} \quad (12)$$

Assuming cellwise discretization for the time derivative and source terms, clearing the integrals of constants, employing Green's theorem on the dispersion term and employing a backwards finite difference approximation for the time derivative and discretization (14) for C, results in

$$\left[\frac{(\varepsilon\rho)_i V_i}{\Delta t_{n+1}}\right](C_i^{n+1}-C_i^n) + \sum_{j=1}^{NN} C_j^{n+1}\int_V [(\varepsilon\rho\mathbf{v})\cdot\nabla\phi_j]\phi_i\, dV + \sum_{j=1}^{NN} C_j^{n+1}\int_V [\varepsilon\rho(D_m\mathbf{I}+\mathbf{D})\cdot\nabla\phi_j]\cdot\nabla\phi_i\, dV = Q_i(C_i^*-C_i)^{n+1} \qquad i=\overline{1, NN} \quad (A13)$$

which may be solved for concentration at all nodes, C_i^{n+1}.

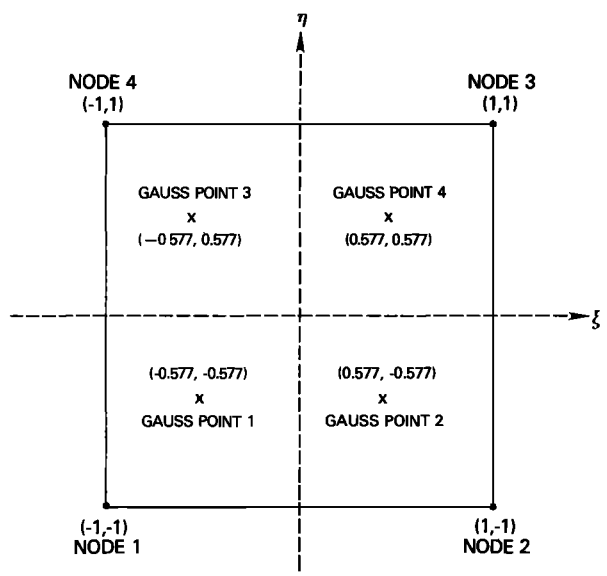

Fig. 18. Finite element in local coordinate system with Gauss points.

The dispersive flux across boundaries has been assumed to be much less than the advective flux in (A13). Integrations are carried out as described above, using densities based on concentration, $C(t_{n+1})$ in relation (2).

The methods of upstream weighting the advective solute flux term or of employing asymmetric rather than Galerkin weighting functions [e.g., *Huyakorn and Pinder*, 1983] are not employed. These methods have been applied to transport models in order to damp spatial oscillations of concentration in meshes which are too coarse. They increase the effective local value of longitudinal dispersivity by a factor proportional to local mesh spacing in the direction of flow. Increasing dispersivity through these complicated methods is computationally expensive. Further, having dispersivity as a function of the numerical discretization size rather than of a physical parameter is confusing when applying a model. A direct adjustment of the longitudinal dispersivity has the equivalent damping effect and is preferable; however, the correct modeling approach for both finite element and finite difference models is to design the mesh fine enough to give nonoscillating solutions at the specified physical value of longitudinal dispersivity.

APPENDIX B: CONSISTENT VELOCITY APPROXIMATIONS

The requirement of consistency is applied in each local direction of isoparametric coordinates, ξ and η, (Figure 18) as follows. First, the ξ component of the density-gravity term in local coordinates must have the same space dependency as the pressure derivative term in local coordinates $\partial p/\partial\xi$ in that direction. Second, the η component of the density-gravity term must vary in space functionally as does $\partial p/\partial\eta$. The basis functions and derivatives are as follows:

$$\Omega_1(\zeta,\eta) = \Xi_- H_- \quad (B1a)$$

$$\Omega_2(\zeta,\eta) = \Xi_+ H_- \quad (B1b)$$

$$\Omega_3(\zeta,\eta) = \Xi_+ H_+ \quad (B1c)$$

$$\Omega_4(\zeta,\eta) = \Xi_- H_+ \quad (B1d)$$

where

$$\Xi_-(\xi) = \tfrac{1}{2}(1-\xi) \quad (B2a)$$

$$\Xi_+(\xi) = \tfrac{1}{2}(1+\xi) \quad (B2b)$$

$$H_-(\eta) = \tfrac{1}{2}(1-\eta) \quad (B2c)$$

$$H_+(\eta) = \tfrac{1}{2}(1+\eta) \quad (B2d)$$

The two-dimensional bilinear basis functions $\phi_i(x, z)$ in (13) and (14) when defined in the local element coordinate system (ξ, η) are denoted as $\Omega_i(\xi, \eta)$, $i = 1, 2, 3, 4$. There is one basis function defined for each node in a quadrilateral element. The derivatives of the bilinear basis functions depend on only one space coordinate:

$$\frac{\partial\Omega_1}{\partial\xi} = -\tfrac{1}{2}H_- \qquad \frac{\partial\Omega_1}{\partial\eta} = -\tfrac{1}{2}\Xi_- \quad (B3a)$$

$$\frac{\partial\Omega_2}{\partial\xi} = +\tfrac{1}{2}H_- \qquad \frac{\partial\Omega_2}{\partial\eta} = -\tfrac{1}{2}\Xi_+ \quad (B3b)$$

$$\frac{\partial\Omega_3}{\partial\xi} = +\tfrac{1}{2}H_+ \qquad \frac{\partial\Omega_3}{\partial\eta} = +\tfrac{1}{2}\Xi_+ \quad (B3c)$$

$$\frac{\partial\Omega_4}{\partial\xi} = -\tfrac{1}{2}H_+ \qquad \frac{\partial\Omega_4}{\partial\eta} = +\tfrac{1}{2}\Xi_- \quad (B3d)$$

The basis function for node i is $\Omega_i(\xi, \eta)$. The pressure gradient within an element in local coordinates is defined in terms of the derivatives with respect to the local coordinates:

$$\frac{\partial p}{\partial \xi}(\xi, \eta) = \sum_{i=1}^{4} p_i \frac{\partial \Omega_i}{\partial \xi} \tag{B4a}$$

$$\frac{\partial p}{\partial \eta}(\xi, \eta) = \sum_{i=1}^{4} p_i \frac{\partial \Omega_i}{\partial \eta} \tag{B4b}$$

The essence of this consistent method is in finding a local discretization of $\rho\mathbf{g}$, with a spatial functionality that is consistent with the local pressure derivatives. This function may be found by inspection to be

$$(\rho g)_\xi^*(\xi, \eta) = \sum_{i=1}^{4} \rho_i g_{\xi_i} \left| \frac{\partial \Omega_i}{\partial \xi} \right| \tag{B5a}$$

$$(\rho g)_\eta^*(\xi, \eta) = \sum_{i=1}^{4} \rho_i g_{\eta_i} \left| \frac{\partial \Omega_i}{\partial \eta} \right| \tag{B5b}$$

where the vertical bars indicate absolute value; ρ_i is the value of ρ at node i in the element based on the value of C at the node through relation (2); g_{ξ_i} is the ξ component of $\mathbf{g}$ at node i; g_{η_i} is the η component of $\mathbf{g}$ at node i; and $(\rho g)_\xi^*(\xi, \eta)$ is the consistent representation of the term for the ξ direction and $(\rho g)_\eta^*(\xi, \eta)$ for the η direction. Note that η dependence is removed for the η term at a given ξ, and ξ dependence is removed from the ξ term for a given η.

This functionality is equivalent to that of the pressure gradient term in each local direction (equations (B4*a*) and (B4*b*)). No particular significance should be attached to the absolute values of basis function derivatives, except that these satisfy the requirements of consistency. This discretization of the (ρg) term (equations (B5*a*) and (B5*b*)) is robust in that it allows both the density and local gravity vector components to vary over an element. The local gravity vector (g_ξ, g_η) required by relations (B5*a*) and (B5*b*) may be obtained for each element by a coordinate transformation:

$$\begin{Bmatrix} g_\xi \\ g_\eta \end{Bmatrix} = [J] \begin{Bmatrix} g_x \\ g_z \end{Bmatrix} \tag{B6}$$

where $[J]$ is the Jacobian matrix defined by

$$[J] = \begin{bmatrix} \frac{\partial x}{\partial \xi} & \frac{\partial z}{\partial \zeta} \\ \frac{\partial x}{\partial \eta} & \frac{\partial z}{\partial \eta} \end{bmatrix} = \begin{bmatrix} \frac{\partial \Omega_1}{\partial \xi} & \frac{\partial \Omega_2}{\partial \xi} & \frac{\partial \Omega_3}{\partial \xi} & \frac{\partial \Omega_4}{\partial \xi} \\ \frac{\partial \Omega_1}{\partial \eta} & \frac{\partial \Omega_2}{\partial \eta} & \frac{\partial \Omega_3}{\partial \eta} & \frac{\partial \Omega_4}{\partial \eta} \end{bmatrix} \begin{bmatrix} x_1 & z_1 \\ x_2 & z_2 \\ x_3 & z_3 \\ x_4 & z_4 \end{bmatrix} \tag{B7}$$

where (x_i, z_i) are the global coordinates of the nodes in the element.

The eight gravity vector components at the nodes in each element need be calculated only once for a given mesh and may be saved at the start of a simulation. The values of the consistent density-gravity terms and pressure derivatives in global coordinates are obtained through another transformation:

$$\begin{Bmatrix} \frac{\partial p}{\partial x} \\ \frac{\partial p}{\partial y} \end{Bmatrix} = [J^{-1}] \begin{Bmatrix} \frac{\partial p}{\partial \xi} \\ \frac{\partial p}{\partial \eta} \end{Bmatrix} \tag{B8}$$

$$\begin{Bmatrix} (\hat{\rho g})_x \\ (\hat{\rho g})_z \end{Bmatrix} = [J^{-1}] \begin{Bmatrix} (\rho g)_\xi \\ (\rho g)_\eta \end{Bmatrix} \tag{B9}$$

where $(\hat{\rho g})_x$ and $(\hat{\rho g})_z$ are the consistently discretized density-gravity term components in global coordinates, and $[J^{-1}]$ is the inverse of the Jacobian matrix.

Acknowledgments. The authors gratefully acknowledge T. Reilly, U.S. Geological Survey, for helping to bring the consistency problem to light; F. Lewis, formerly of U.S. Geological Survey, for analyzing the *Elder* [1961] problem; and the research group headed by E. Buetow, Technical University of Berlin, for suggesting the Elder problem as a test case.

REFERENCES

Bear, J., *Hydraulics of Groundwater*, 567 pp., Mc-Graw Hill, New York, 1979.

Bennett, G. D., M. J. Mundorff, and S. A. Hussain, Electric-analog studies of brine coning beneath fresh-water wells in the Punjab Region, West Pakistan, *U.S. Geol. Surv. Water Supply Pap., 1608-J*, pp. J1–J31, 1968.

Desai, C. S., and D. N. Contractor, Finite element analysis of flow, diffusion and salt water intrusion in porous media, in *Formulation and Computational Algorithms in Finite Element Analysis*, edited by K. J. Bathe et al., pp. 958–983, MIT, Cambridge, Mass., 1977.

Elder, J. W., Numerical experiments with free convection in a vertical slot, *J. Fluid Mech., 24*(4), 823–843, 1966.

Elder, J. W., Transient convection in a porous medium, *J. Fluid Mech., 27*(3), 609–623, 1967.

Frind, E. O., Simulation of long-term transient density-dependent transport in groundwater, *Adv. Water Resour., 5*, 73–78, 1982*a*.

Frind, E. O., Seawater intrusion in continuous coastal aquifer-aquitard systems, *Adv. Water Resour., 5*, 89–97, 1982*b*.

Frind, E. O., The principal direction technique: A new approach to groundwater contaminant transport modeling, in *Finite Elements in Water Resources*, edited by Holz et al., pp. 13/25-13/42, Springer-Verlag, New York, 1982*c*.

Henry, H. R., Effects of dispersion on salt encroachment in coastal aquifers, *U.S. Geol. Surv. Water Supply Pap., 1613-C*, pp. C71–C84, 1964.

Huyakorn, P. S., and G. F. Pinder, *Computational Methods in Subsurface Flow*, 473 pp., Academic, Orlando, Fla., 1983.

Huyakorn, P. S., and C. Taylor, Finite element models for coupled groundwater flow and convective dispersion, *Finite Elements in Water Resources*, edited by Gray et al., pp. 1.131–1.151, Pentech, London, 1976.

INTERA, Revision of the documentation for a model for calculating effects of liquid waste disposal in deep saline aquifers, *U.S. Geol. Surv. Water Resour. Invest. Rep., 79-96*, 73 pp., 1979.

Lebbe, L. C., Mathematical model of the evolution of the fresh water lens under the dune and beach with semi-diurnal tides, *Geol. Appl. Idrogeol., 18*(2), 211–266, 1983.

Lee, C-H., and R. T. Cheng, On seawater encroachment in coastal aquifers, *Water Resour. Res., 10*(5), 1039–1043, 1974.

Mink, J. F., State of the groundwater resources of Southern Oahu, technical report, 83 pp., Board of Water Supply, City and County of Honolulu, Hawaii, 1980.

Neuman, S. P., Effect of partial penetration on flow in unconfined aquifers considering delayed gravity response, *Water Resour. Res., 10*(2), 303–311, 1974.

Pinder, G. F., and H. H. Cooper, A numerical technique for calculating the transient position of the saltwater front, *Water Resour. Res., 6*(3), 875–882, 1970.

Pinder, G. F., and W. G. Gray, *Finite Element Simulation in Surface and Subsurface Hydrology*, 295 pp., Academic, Orlando, Fla., 1977.

Reilly, T. E., and A. S. Goodman, Quantitative analysis of saltwater-freshwater relationships in groundwater systems—A historical perspective, *J. Hydrol., 80*, 125–160, 1985.

Reilly, T. E., and A. S. Goodman, Analysis of saltwater upconing beneath a pumping well, *J. Hydrol., 89*, 169–204, 1987.

Segol, G., and G. F. Pinder, Transient simulation of saltwater intrusion in southeastern Florida, *Water Resour. Res., 12*(1), 65–70, 1976.

Segol, G., G. F. Pinder, and W. G. Gray, A Galerkin finite element technique for calculating the transient position of the saltwater front, *Water Resour. Res., 11*(2), 343–347, 1975.

Souza, W. R., and C. I. Voss, Analysis of an anisotropic coastal aquifer system using variable density flow and solute transport simulation, *J. Hydrol., 92*, 17–41, 1987.

Visher, F. N., and J. F. Mink, Ground-water resources in southern Oahu, Hawaii, *U.S. Geol. Surv. Water Supply Pap., 1778*, 133 pp., 1964.

Volker, R. E., Comparison of immiscible and miscible fluid models for sea water intrusion in aquifers, paper presented at Proceedings, 7th Australian Hydraulics and Fluid Mechanics Conference, Inst. of Eng., Brisbane, Qld., 1980.

Volker, R. E., and K. R. Rushton, An assessment of the importance of some parameters for seawater in trusion in aquifers and a comparison of dispersive and sharp-interface modelling approaches, *J. Hydrol., 56*, 239–250, 1982.

Voss, C. I., SUTRA: A finite-element simulation model for saturated-unsaturated fluid-density-dependent ground-water flow with energy transport or chemically-reactive single-species solute transport, *U.S. Geol. Surv. Water Resour. Invest. Rep., 84-4369*, 409 pp., 1984.

W. R. Souza, U.S. Geological Survey, Box 50166, Honolulu, HI 96850.

C. I. Voss, U.S. Geological Survey, 431 National Center, Reston, VA 22092.

(Received September 10, 1986;
revised June 10, 1987;
accepted June 19, 1987.)